

Optimizing line-plot size for personal laser scanning: modeling distance-dependent tree detection probability along transects

Tim Ritter,
Andreas Tockner,
Ralf Krassnitzer,
Sarah Witzmann,
Christoph Gollob,
Arne Nothdurft

Personal laser scanning (PLS) systems are gaining popularity in forest inventory research and practice. They are primarily utilized on circular or compact rectangular sample plots to mitigate potential instrument drift and enhance tree detection rates, and a closed-loop scan path is usually implemented to achieve these objectives, ensuring thorough coverage of the plot. This study introduced a novel approach by applying the distance-sampling framework to PLS data collected during walks along line transects. Modeling the distance-dependent probability of tree detection using PLS coupled with automatic routines for point cloud processing aimed to ascertain the optimal width of line-plots to maximize tree detection rates. The optimized plots exhibited tree detection rates exceeding 99%, which facilitated accurate estimates of tree density, basal area, and growing stock volumes. This proposed method demonstrated considerable potential for data collection while walking along line transects in forests. For instance, the otherwise unproductive working time of field crews moving between systematically arranged sample plots can be utilized for additional data collection without generating additional costs. This innovative approach not only enhances operational efficiency but also establishes a foundation for further advancements to explore PLS applications in forest management practices.

Keywords: Personal Laser Scanning, Lidar, Forest Inventory, Distance Sampling, Line Transect Sampling, Tree Detection

Introduction

Forest inventories provide means and totals for measuring forest characteristics, such as the volume of growing stock, area of a certain forest type, and volume of dead wood or vegetation (Kangas et al. 2006), which are crucial for decision-making in forest management (Penman et al. 2003). The Swedish botanist and forestry researcher Israel af Ström introduced systematic strip sampling in the 1830s and conducted the first regional-scale forest inventories, which remained popular for almost a century (Kangas et al. 2006). National forest inventories (NFIs) based on modern statistical principles were implemented in Norway, Finland, and Sweden in 1919, 1920, and 1923 (Kershaw et al. 2016). In these NFIs, systematic strip sampling was replaced by a line-plot system wherein

relatively small plots can be sampled along systematically arranged lines (Kangas et al. 2006, Tokola 2006, Tomppo 2006). Around 1990, many countries redesigned their NFIs and implemented systematic grid-based sample designs, consistent plot designs, and re-measurement intervals (Kershaw et al. 2016) that are still commonly used today.

Surprisingly, the instruments used in NFIs have changed marginally in recent decades, and mechanical and optical instruments, such as calipers, hypsometers, relascopes, and tape measures, are still commonly used today (Kauffman et al. 2017, Kershaw et al. 2016, Köhl & Magnussen 2016), although their usage is often labor-intensive and prone to measurement errors (Liang et al. 2016, 2018, Ritter et al. 2017).

Terrestrial laser scanning (TLS) can collect high-resolution 3-dimensional (3D) data and represent stems and branches comprehensively; therefore, TLS-based estimates of tree attributes have reached an accuracy level that surpasses conventional measures (Witzmann et al. 2022). Despite these obvious advantages, TLS has so far hardly been used in forest inventory practices because the scanners are too heavy and complex to use (Mokroš et al. 2021). In addition to the pure scanning time, a substantial amount of working time is used to set up the scanner at different positions within a sample plot and to install artificial reference targets for co-registration of the scans (Gollob et al. 2019). Personal laser scanning (PLS) systems overcome these limitations by enabling scanning during motion and registering point clouds using simultaneous localization and mapping algorithms (Gollob et al. 2020). Consequently, the PLS point clouds are often noisier and less precise than the TLS point clouds (Bauwens et al. 2016, Chen et al. 2019). However, they can derive accurate estimates of tree-level attributes from these datasets (Tockner et al. 2022).

A major challenge in laser scanning operations is occlusion, which leads to incomplete point clouds (Dassot et al. 2011) and consequently to the non-detection of several trees. The problem is especially pronounced when TLS is used in the single-scan mode (Ritter et al. 2020), but also oc-

□ University of Natural Resources and Life Sciences, Vienna - BOKU, Department of Forest and Soil Science, Institute of Forest Growth, Vienna (Austria)

@ Tim Ritter (tim.ritter@boku.ac.at)

Received: Feb 15, 2024 - Accepted: Jul 26, 2024

Citation: Ritter T, Tockner A, Krassnitzer R, Witzmann S, Gollob C, Nothdurft A (2024). Optimizing line-plot size for personal laser scanning: modeling distance-dependent tree detection probability along transects. *iForest* 17: 269-276. - doi: [10.3832/ifor4588-017](https://doi.org/10.3832/ifor4588-017) [online 2024-09-07]

Communicated by: Marco Borghetti

curs in the multi-scan mode (Gollob et al. 2019, Liang et al. 2016, Ritter et al. 2020). In PLS applications, occlusion strongly depends on the scanning path and scan density (Bauwens et al. 2016, Del Perugia et al. 2019, Tupinambá-Simões et al. 2023). Bauwens et al. (2016) recommended that the PLS path should end at the starting point (thereby creating a “closed loop”) to minimize instrumental drift and provide good coverage of the sample plot with minimum occlusion and range noise. Following these recommendations for the scan path layout, PLS was limited to relatively small and compact sample plots and experimental stands. Thus, in the forest inventory context, PLS has so far been used nearly exclusively in this setting type.

However, PLS principally allows data collection while walking along linear transects and can thus be used in a line-plot sampling system, which has rarely been used in recent years. However, in typical modern systematic grid-based sample systems, field crews walk along linear paths, for instance, when moving from one sample plot to the other, and no data are collected while walking. Thus, PLS principally provides the opportunity to collect data between sample plots without increasing the workload, simply by switching on the PLS scanner and carrying it from one sample point to another along a path that must be walked. However, this scanning layout violates all the recommendations on good PLS practices outlined above, and the non-detection of trees may become a serious challenge that must be carefully addressed.

Non-detection of sample objects is a common problem in wildlife ecology; thus, a distance sampling framework (Buckland et al. 2001, 2004) was developed for applications in this field (Thomas et al. 2012). The main objective of distance sampling is to use the observed distances between the observer and detected objects of interest to fit a detection function that describes the decrease in detectability with increasing distance (Thomas et al. 2012). In the forest inventory context, distance sam-

pling has been successfully used for sampling deadwood (Ritter & Saborowski 2012, 2014), habitat trees (Bäuerle & Nothdurft 2011, Didas 2009), and low-abundance tree species (Kissa & Sheil 2012), and to correct non-detection in angle-count sampling (Ritter et al. 2013), single-scan TLS (Astrup et al. 2014, Ducey & Astrup 2013), and multi-scan TLS (Ritter et al. 2020, 2021).

In this study, the potential of PLS-based data collection along lines was evaluated regarding the possibility of collecting additional data during systematic grid-based forest inventories using the walking time for PLS scans and without spending any additional working time on other plots in the field. To the best of our knowledge, this is the first study to adopt the distance-sampling framework for PLS data. We used a GeoSLAM ZEB Horizon® (GeoSLAM Ltd., Nottingham, UK) PLS system to collect data along 23 transects with a total length of 4157.7 m in two stands that were fully mapped for reference. Three different detection functions were evaluated, a correction for non-detection was developed, and recommendations for an optimal line-plot width were also made.

The main objectives of this study were to (i) test the applicability of PLS along transects, (ii) determine the optimal width of line plots to maximize tree detection rates with PLS using the distance sampling framework, and (iii) optimize line plot length to facilitate precise estimates of tree density, basal area, and growing stock volume.

Materials and methods

Experimental stands and reference data

The survey was conducted at two fully mapped experimental stands (Fig. 1). Position, diameter at 1.3 m height (dbh), and height of all trees having a dbh \geq 5 cm were manually measured for reference. Reference stem volume was calculated using an established stem form function (Pollanschütz 1965) with height and dbh as input variables.

The first experimental stand with an area of 4.88 ha located near the village of Kreisbach, Lower Austria (48.10° N, 15.63° E), was referred to as “BuLae”. The stand was mature and characterized by an uneven mixture of 90% beech (*Fagus sylvatica*) and 6% larch (*Larix decidua*), with no understory and only sparse natural regeneration. The mixed tree species included 2% spruce (*Picea abies*), 1% oak (*Quercus* spp.), and less than 1% other species, mainly fir (*Abies alba*), hornbeam (*Carpinus betulus*), lime (*Tilia* spp.), and ash (*Fraxinus excelsior*). The total number of trees was 2867 corresponding to a density of 588.5 trees ha⁻¹. The median tree height was 30.2 m (min = 3.4 m, max = 43.5 m), and the median dbh was 29.3 cm (min = 5.0 cm, max = 68.0 cm). Stand basal area was 216.1 m² (= 44.3 m² ha⁻¹) and total volume of the growing stock was 3203.3 m³ (= 656.4 m³ ha⁻¹).

The second experimental stand with an area of 4.08 ha located in the BOKU University training forest near Hochwolkersdorf Village in Lower Austria (47.68° N, 16.29° E) was referred to as “30k”. This stand included 1789 trees, with a corresponding density of 438.5 trees ha⁻¹. The stand is characterized by high structural diversity, including a spatially irregularly distributed understory and regeneration. Diversity of tree species was comparatively high for the area, with 38% spruce (*Picea abies*), 38% beech (*Fagus sylvatica*), 15% fir (*Abies alba*), 5% pine (*Pinus sylvestris*), 4% larch (*Larix decidua*), and <1% of other broadleaf species. Natural regeneration occurred in irregularly arranged clusters comprising approximately 90% beech and 10% fir. The median tree height was 29.7 m (min = 5.4 m, max = 40.9 m), and the median dbh was 36.3 cm (min = 9.9 cm, max = 67.3 cm). Stand basal area was 191.5 m² (= 46.9 m² ha⁻¹) and the total volume of the growing stock was 2686.7 m³ (= 658.8 m³ ha⁻¹).

Scan data collection and analysis

Scan data collection was performed under defoliated conditions in winter 2021/22 using a GeoSLAM ZEB Horizon® (GeoSLAM Ltd., Nottingham, UK) PLS system that uses the simultaneous localization and mapping technique. The scanner has a maximum range of 100 m and collects 300,000 scan points s⁻¹ with an accuracy of \pm 6 mm (GeoSLAM 2023b).

The transects were aligned parallel to each other, with a spacing of approximately 20 m. The start and end points of each transect were located on opposing stand borders (open loops). Nine transects were scanned in BuLae, having a mean length of 284.3 m (minimum length = 122.6 m, maximum length = 461.0 m), and 14 transects were scanned in 30k, having a mean length of 115.5 m (minimum length = 102.7 m, maximum length = 130.0 m). The transect lengths resembled the typical distances between forest inventory sample points.

The raw scan data were converted into

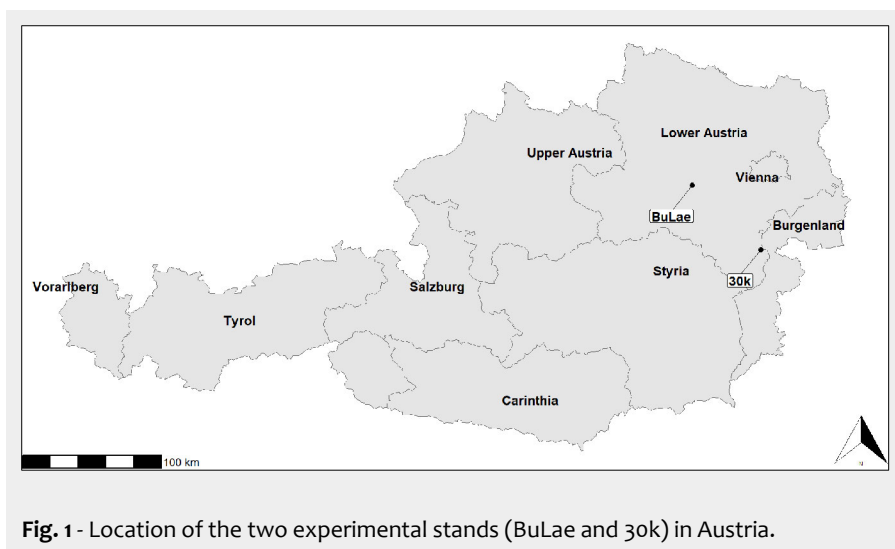


Fig. 1 - Location of the two experimental stands (BuLae and 30k) in Austria.

point clouds in the .laz format using the software GeoSlam HUB ver. 5.3 (GeoSLAM 2023a) in a local coordinate reference system for each transect separately (Fig. 2). In addition to the point cloud, the trajectory of the instrument (*i.e.*, walking path of the observer) was exported in the .csv format with the same coordinate reference system as the corresponding point cloud. The point clouds were then processed in R language and environment for statistical computing (R Core Team 2022) using fully automatic routines for tree detection, tree segmentation, and tree variable estimation implemented in the R-package “treeX” (Tockner 2024). In a preparatory step, the point cloud was cropped, normalized, and filtered, leaving only vegetation hits. Tree positions were then automatically detected through multi-stage, density-based clustering, and the diameter at breast height was estimated by fitting a circle to the trunk cross-section at a height of 1.3 m (Ritter et al. 2017, Gollob et al. 2020). The point cloud was then voxelated and the detected tree positions served as starting points for a 3D region-growing algorithm for automatic tree segmentation (Tockner et al. 2022), allowing the height of each individual tree to be estimated as the difference between the highest and lowest z-values of voxels belonging to the tree. The tree volume was then estimated using the same stem form function (Pollanschütz 1965) as the reference data to ensure a fair comparison. Finally, trees with dbh < 5 cm were removed from the tree list, as this was also the caliper threshold in the reference data.

Orthogonal distances between the tree positions and the transect were calculated, and distance sampling analysis was conducted using the R package “Distance” version 1.0.7. (Miller et al. 2019).

Distance sampling approach

We used the classic line transect sampling approach of the distance sampling framework to estimate the number of trees per unit area. A brief description of the procedure is given below, for more details we refer to Buckland et al. (2001, 2004).

Using the classic line-plot sampling approach, *m* number of plots with a constant width 2ω were sampled along a line. With l_i being the length of the *i*-th plot, the total length of all plots was then $L = \sum_{i=1}^m l_i$. Thus, all *n* trees within an area of size $a = 2\omega L$ were sampled, and the density *D*, *i.e.*, the number of trees per area unit, was estimated using the following equation (eqn. 1):

$$\hat{D} = \frac{n}{2\omega L} \tag{1}$$

However, this implied perfect detectability of trees, and any missed trees will lead to a non-detection bias. Using laser scanning systems and automatic routines for tree detection, the probability of detecting a tree decreases with increasing distance between the scanner and the tree, owing

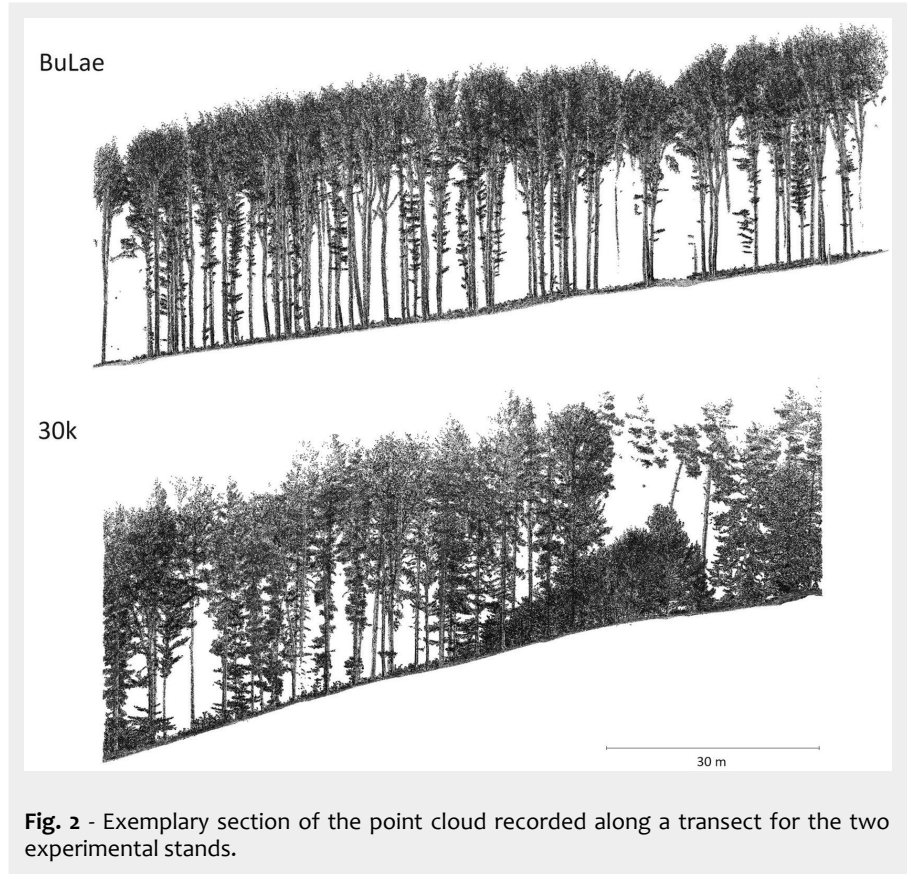


Fig. 2 - Exemplary section of the point cloud recorded along a transect for the two experimental stands.

to decreasing point density and obstruction (Astrup et al. 2014, Ducey & Astrup 2013, Ritter et al. 2020, 2021). Thus, only a proportion P_a of the trees located within an area of size *a* was detected. If P_a can be estimated by \hat{P}_a , *D* can be estimated as follows (eqn. 2):

$$\hat{D} = \frac{n}{2\omega L \hat{P}_a} \tag{2}$$

But how can P_a be estimated? According to Buckland et al. (2001), the basic concept of line transect sampling is that the detectability of objects decreases with increasing distance *x* between the transect and the object of interest (a tree in our application). By fitting a distance-dependent detection function *g(x)* to the normalized detection of objects located directly on the transect [$g(0) = 1$], the mean detection probability within a strip of area *a* can then be estimated as (eqn. 3):

$$\hat{P}_a = \frac{\int_0^{\omega} g(x) dx}{\omega} \tag{3}$$

The density estimator (eqn. 2) then becomes (eqn. 4):

$$\hat{D} = \frac{n}{2L \int_0^{\omega} g(x) dx} \tag{4}$$

The standard error of \hat{D} , can be estimated using the delta method as described below (Seber 1982 - eqn. 5):

$$SE(\hat{D}) = \sqrt{\hat{D}^2 \cdot \left(\frac{\widehat{var}(n)}{n^2} + \frac{\widehat{var}(a \cdot \hat{P}_a)}{(a \cdot \hat{P}_a)^2} \right)} \tag{5}$$

The detection function *g(x)* is typically represented by a parametric function and can be fitted using maximum-likelihood techniques (Buckland et al. 2001, 2004). Because parametric detection functions have proven to be robust and provide sufficient flexibility, and because their inference is straightforward, they are generally preferred over nonparametric alternatives (Quang 1993).

The best detection function was selected from nine candidate functions based on the minimum Akaike Information Criterion (AIC), for both stands separately. The candidate functions comprised a key function and a first-order series expansion (Tab. 1).

The distance sampling approach allowed the correction of the number of missed trees and provided estimates for the number of trees per unit area. However, forest managers are normally more interested in stand basal area (BA) and volume of growing stock (V). As tree size can possibly affect detection probability, larger trees might be overrepresented in the sample (size bias); therefore, estimates of BA and V derived from the distance sample might also be biased. The size bias can be principally corrected using regression techniques (Buckland et al. 2001, Ritter & Saborowski 2012); however, this introduces a new source of uncertainty. Moreover, this approach only provides estimates for the totals of BA and V but no single-tree informa-

Tab. 1 - Combinations of key functions and series expansions used as candidate models for estimating the detection function. ω is the scale parameter of the detection function, b is the shape parameter of the detection function, y is the coefficient of the series expansion, H_j is the j^{th} Hermite polynomial, and a_j is set to zero if term j is not used in the model.

Key function	Series expansion
Uniform: $\hat{g}(x) = 1/\omega$	None Cosine: $\sum_{j=1}^m a_j \cdot \cos(j\pi y/\omega)$ Simple polynomial: $\sum_{j=1}^m a_j (y/\omega)^{2j}$
Half-normal: $\hat{g}(x) = \exp(-(x^2/2\sigma^2))$	None Cosine: $\sum_{j=2}^m a_j \cdot \cos(j\pi y/\omega)$ Hermite polynomial: $\sum_{j=1}^m a_j H_{2j}(y/\sigma)$
Hazard-rate: $\hat{g}(x) = 1 - \exp(-(x/\sigma)^b)$	None Cosine: $\sum_{j=2}^m a_j \cdot \cos(j\pi y/\omega)$ Hermite polynomial: $\sum_{j=1}^m a_j H_{2j}(y/\sigma)$

tion. Therefore, we did not follow this approach and instead used the shape of the detection function to determine the optimal line-plot width, that is, the maximum line-plot width where tree detection is certain and non-detection becomes irrelevant.

Determination of optimal line-plot size

Detection functions often show a noticeable shoulder, i.e., a range of distances from the line for which the slope $g'=0$. Thus, the shoulder indicates the range of distances at which a tree can be detected with certainty (Prieto Gonzalez et al. 2017). We used this characteristic to estimate the optimal line-plot width, i.e., the maximum plot width for which the detectability of trees is certain, by determining the greatest distance ω_{opt} where $g' < 0.005$. We used this constraint instead of $g'=0$ because the numerically calculated values of $g'(x)$ might have been influenced by the rounding errors of the parameter estimates. The corresponding optimal line-plot width was then estimated as $2\omega_{opt}$, because trees could be detected on the left and right side of the line. We then truncated the distance sampling data at ω_{opt} , such that every transect could be treated as a line-plot of area $a_i = 2\omega_{opt} l_i$.

As the sampling units are of unequal size ($a_i \neq const$), the population mean of any re-

sponse variable Y (D, BA, V) cannot be estimated as the sample mean over the m line-plots because the observations y_i are correlated with a_i . Thus, we estimated the population mean of any response variable per unit area \hat{Y}_R using the following ratio estimator (eqn. 6):

$$\hat{Y}_R = \frac{\sum_{i=1}^m y_i}{\sum_{i=1}^m a_i} \tag{6}$$

where \hat{Y}_R is model unbiased only in case of a linear relationship of the form $y_i = \beta a_i + \epsilon_i$ between y and a , where the regression line is passing through the origin with positive slope β , and the random error ϵ_i is independently and identically normal distributed. Otherwise, \hat{Y}_R is approximately unbiased for sufficiently large sample sizes (Cochran 1977, De Vries 1986).

Using the finite population approach, the standard error (SE) for \hat{Y}_R was estimated as (eqn. 7):

$$SE(\hat{Y}_R) = \sqrt{\frac{1-f}{m \cdot \bar{a}} \cdot (s_y^2 + \hat{Y}_R^2 s_a^2 - 2\hat{Y}_R s_{ay})} \tag{7}$$

where f is the sampling fraction, \bar{a} is the mean line-plot area, s_y^2 is the sample variance of the target variable over line-plots, s_a^2 is the sample variance of the line-plot areas, and s_{ay} is the covariance between the line-plot area and the target variable (Coch-

ran 1977). As the term $m \cdot \bar{a} = const$ for any given value of f , m has no direct influence on the estimated SE. However, s_y^2 and s_{ay} depend on the distribution of line-plot sizes a_i , and therefore, for a fixed sampling fraction f , also on m .

To assess the impact of different lengths and numbers of line-plots at a constant sampling fraction, we divided the individual transects into segments ranging from 1 to 50 m in length. Segments at the stand edges may have been shorter because of the irregular shape of the stands. To capture the effect of different starting points on segmentation, the starting points were varied on a 1×1 m grid.

Accuracy of tree detection

Eqn. 6 and eqn. 7 yield (approximately) unbiased estimates only when all trees within the sample plots are detected and no false detection occurs. Although the distance-sampling model indicated total detectability within the plot, it did not provide any false detection information. Thus, the accuracy of the tree detection was evaluated by comparing the automatically detected tree positions with the reference data. The automatically detected tree positions were assigned to the reference positions using a point assignment algorithm (Hyypä et al. 2021, Witzmann 2022), with position deviations of up to 0.5 m permitted. We then assessed the accuracy of tree detection in terms of the omission error, o (eqn. 8), commission error c (eqn. 9), and overall accuracy acc (eqn. 10) to evaluate the accuracy of the model prediction and the assumption that there were no false-positive detections:

$$o(\%) = \left(1 - \frac{n_{match}}{n_{ref}}\right) \cdot 100 \tag{8}$$

$$c(\%) = \frac{n_{falsepos}}{n_{extr}} \cdot 100 \tag{9}$$

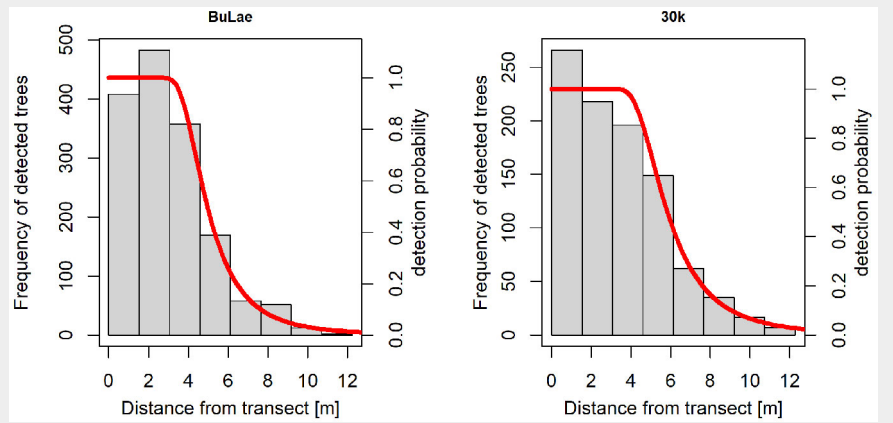
$$acc(\%) = 100\% - (o(\%) + c(\%)) \tag{10}$$

where n_{match} is the number of correctly found reference trees, n_{ref} is the total number of reference trees, $n_{falsepos}$ is the number

Tab. 2 - Akaike information criterion (AIC) and parameter estimates for the different candidate detection functions and experimental stands. Emphasized: The hazard rate detection function that was finally selected.

Detection function	BuLae				30k			
	AIC	σ	b	SEcoef	AIC	σ	b	SEcoef
Uniform	7728.2	NA	NA	NA	4654.5	NA	NA	NA
Uniform + Cosine	6371.1	NA	NA	0.998	4106.3	NA	NA	0.979
Uniform + Polynomial	7127.7	NA	NA	-0.997	4439.1	NA	NA	-0.994
Half-normal	6230.7	3.664	NA	NA	4085.6	4.241	NA	NA
Half-normal + Cosine	6217.9	3.400	NA	-0.219	4085.4	4.124	NA	-0.096
Half-normal + Polynomial	6219.6	2.878	NA	-0.270	4087.1	4.356	NA	-0.359
Hazard rate	6198.7	4.558	4.363	NA	4084.8	5.360	4.276	NA
Hazard rate + Cosine	6200.7	4.558	4.363	0.000	4087.0	6.021	5.284	0.203
Hazard rate + Polynomial	6199.3	4.483	3.783	0.342	4086.6	5.665	3.628	0.228

Fig. 3 - Hazard rate detection function (red line) fitted to the histogram of detected tree frequency in the different distance classes.



of tree positions which could not be assigned to an existing tree in the reference data, and n_{extr} is the number of automatically detected tree positions ($n_{match} + n_{false-pos}$). The omission error o (%) measures the percentage of undetected trees, commission error c (%) measures the percentage of falsely detected tree locations, and overall accuracy acc (%) is a combination of the latter two metrics and represents a global quality criterion. The detection rate, measuring the percentage of correctly identified trees, is given by $d_r = 100\% - o$ (%).

Results

Distance sampling approach

All candidate functions were fitted to the observed distances between trees and transects obtained from the PLS data and compared in terms of the minimum AIC.

The detection functions with the hazard rate key generally performed the best for both stands; however, their advantage over the other functions was much more pronounced for BuLae than for 30k. While the uniform detection functions performed clearly inferiorly to the hazard rate functions in both stands, the half-normal detection functions almost reached the AIC level of the hazard rate functions in 30k, whereas they were clearly inferior in BuLae (Tab. 2).

Adding polynomial or cosine series expansions did not result in better performance of the hazard rate function. Thus, the hazard rate detection function without series expansion and with parameter estimates according to Tab. 2 was selected as the final model based on the minimum AIC for both experimental stands. The function showed a strong shoulder for both stands (Fig. 3) ranging from 0 m to approximately 3 m, followed by a steep decline to approximately 8 m. For greater distances, the function asymptotically approached the x-axis.

The estimated tree densities (eqn. 4) ± SE (eqn. 5) was 556.9 ± 18.8 trees ha⁻¹ for BuLae, and 462.7 ± 52.0 trees ha⁻¹ for 30k. The corresponding reference values of 587.5 and 438.5 trees ha⁻¹ were within the respective confidence intervals of the estimates

(Tab. 3). The relative standard error was 9.3% for BuLae and 4.1% for 30k.

Volume and basal area were not estimated with this approach for the reasons explained above (section “Distance sampling approach”).

Line-plot approach

The width of the detection function shoulder was numerically determined as the greatest distance ω_{opt} where $g'(\omega_{opt}) = 0.005$. The closed-form derivative (eqn. 11) existed for the hazard rate function, such that g' was determined without further numerical approximation:

$$g'(x) = \frac{b}{s} \left(\frac{x}{s}\right)^{-b-1} \cdot e^{-\left(\frac{x}{s}\right)^{-b}} \quad (11)$$

The greatest distance ω_{opt} was 2.86 m for BuLae and 3.33 m for 30k. Consequently, line-plots of width $2\omega_{opt}$ (5.72 m for BuLae and 6.66 m for 30k) were observed along the transect lines.

With the given sampling fraction, the mean standard error for the target variable V was minimal for line-plot lengths of 9 m for BuLae and 12 m for 30k (Fig. 4).

Consequently, line-plots of size 9×5.72 m and 12×6.66 m were used to assess the precision of the target variable estimates for BuLae and 30k respectively.

For BuLae, target variable estimates were 571.9 trees ha⁻¹ for density, 45.76 m³ ha⁻¹ for basal area, and 642.7 m³ ha⁻¹ for volume, while for 30k, the estimates were 571.9

Tab. 3 - Tree density, reference values (Ref), estimates (Est), standard errors (SE), and 95% confidence intervals (95%-CI) for both stands.

Stand	Metric	Ref	Est	SE	95%-CI
BuLae	Total number of trees in the stand	2867.0	2717.5	253.9	[2198.2-3359.5]
	Number of trees ha ⁻¹	587.5	556.9	52.0	[450.5-688.4]
30k	Total number of trees in the stand	1789.0	1887.7	76.7	[1737.5-2050.9]
	Number of trees ha ⁻¹	438.5	462.7	18.8	[425.9-502.7]

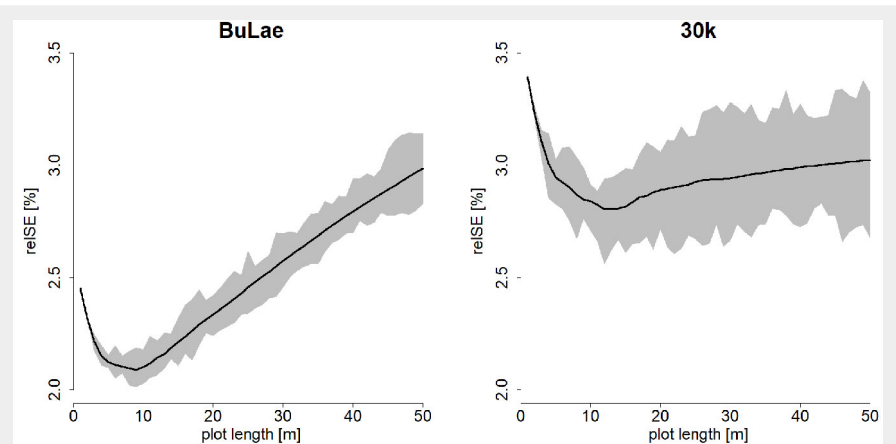


Fig. 4 - Relative standard error (relSE) for the estimated volume per ha V depending on the individual line-plot length. Total line-plot length was constant (2558.7 m for BuLae and 1617 m for 30k). The solid black line indicates the mean relSE for the corresponding plot length, while the gray area indicates the variability of relSE estimates based on the starting point of the systematic grid.

Tab. 4 - Point estimates (Est), reference values (Ref), standard errors (SE), and 95% confidence intervals (95%-CI) for both stands, and for three target variables *D* (trees ha⁻¹), *BA* (Basal area m² ha⁻¹), and *V* (Volume, m³ ha⁻¹). (N): number of plots.

Stand	Plot size (m)	N	Response variable	Ref	Est	SE	95%-CI
BuLae	9 × 5.72	294	<i>D</i> (trees ha ⁻¹)	587.5	571.9	11.3	[553.3-590.4]
			<i>BA</i> (Basal area, m ² ha ⁻¹)	44.28	45.76	0.96	[44.18-47.34]
			<i>V</i> (Volume, m ³ ha ⁻¹)	656.4	642.7	12.9	[620.5-664.8]
30k	12 × 6.66	149	<i>D</i> (trees ha ⁻¹)	438.5	456.7	13.7	[434.1-479.3]
			<i>BA</i> (Basal area, m ² ha ⁻¹)	46.94	45.77	1.28	[43.65-47.89]
			<i>V</i> (Volume, m ³ ha ⁻¹)	658.8	650.6	18.2	[620.5-680.7]

trees ha⁻¹ for density, 45.76 m² ha⁻¹ for basal area, and 642.7 m³ ha⁻¹ for volume. Reference values of all target variables were within the corresponding 95% confidence interval for each experimental stand (Tab. 4). The precision of the estimates was substantially higher for BuLae than for 30k (Tab. 4).

Accuracy of tree detection

The accuracy of target variable point estimates (Tab. 4) depended on the assumption that trees within line-plots of width $2\omega_{opt}$ were detected with certainty, as indicated by the distance sampling model.

To evaluate the validity of the model results, the accuracy of tree detection was assessed based on reference data (Tab. 5). The true detection rates exceeded 99% for both stands (omission errors <1%), and the number of false detections was negligible (commission errors <0.4%). The overall accuracies were 98.88% for BuLae and 98.83% for 30k.

Discussion

Accuracy and precision of forest inventory target variable estimates

The classic line transect sampling approach is primarily designed to estimate detection probability and tree density. We used this approach and achieved a standard error of 52.0 trees ha⁻¹ for BuLae and 18.8 trees ha⁻¹ for 30k (Tab. 3). Contrastingly, the optimized line-plot sampling technique demonstrated a notable reduction in standard errors, resulting in values of 11.3 and 13.7 trees ha⁻¹ for BuLae and 30k, respectively (Tab. 4). This improvement can be attributed to the ability of the meth-

od to precisely estimate the strip width where detection is certain, leveraging the precise measurement of the width of the shoulder of the detection function. Conversely, the conventional approach struggles to model the decrease in detectability with increasing distance from a line with the same level of precision.

The point estimates obtained using the optimized line-plot sampling for the forest inventory target variables (Tab. 4) were approximately unbiased for two reasons: (i) the residuals from the linear models between y_i and a_i and are not independently and identically distributed, rendering eqn. 6 only approximately unbiased; (ii) the detectability of trees in the optimized line-plots was not perfect (Tab. 5) with <1% of the trees missed, thereby introducing a minor negative bias.

The precision of the point estimates for the forest inventory target variables was greater for BuLae than for 30k stand plot. This finding was expected, considering that 30k possesses a more intricate stand structure than BuLae, and that the sampling fraction was higher in BuLae than in 30k.

The open loop scan path did not cause any problems regarding instrumental drift on the observed transects of length varying between 102.7 and 461.0 m, and tree detection was almost perfect on line-plots with optimized width.

The sampling fraction was very high in both stands. In 30k, the total length of the 14 transects was 1617.0 m, and the line-plot width was 6.66 m, yielding a total sample plot area of 10.769 m², or 26.4% of the total stand area (4.08 ha). In BuLae, the total length of the 9 transects was 2558.7 m, and the line-plot width was 5.72 m, yielding a total sample plot area of 14.636 m², or 30.0% of the total stand area (4.88 ha). This high sampling fraction is infeasible in most practical applications. However, providing an efficient methodology for obtaining standard-level volume estimates was not the focus of this study. Instead, we only used the two experimental stands for a comprehensive reference and focused on the potential of PLS-based data collection along lines with regard to the possibility of collecting additional data during systematic grid-based forest inventories. This topic has been further discussed below.

Algorithms for point cloud processing

The distance-sampling approach assumes the total detectability of trees in close proximity to the line transect. However, depending on the algorithms applied for point-cloud processing and tree detection, trees that are visible in the point cloud may remain undetected. For example, the lower part of the stem could be obstructed by natural regeneration or other vegetation types (omission errors). Conversely, algorithms may misinterpret non-tree objects as trees, such as when the branches of fallen trees are oriented vertically (commission error).

This study did not focus on algorithm development, improvement, or comparison of different algorithms. Instead, the emphasis was on applying PLS to an operational setting. Therefore, we utilized a single set of existing algorithms for data analysis. The omission and commission error rates achieved with these algorithms on the line-plots provided very little room for improvement, given that detectability was nearly perfect (>99%) and commission errors were negligible (<0.5%). However, alternative algorithms for point cloud processing can yield detection functions with a broader shoulder, allowing for the sampling of wider line-plots, which is desirable.

Selection of detection function

Parametric detection functions are typically favored over nonparametric alternatives owing to their robustness, sufficient flexibility, and straightforward inferential procedures (Quang 1993). Hence, we exclusively employed parametric candidate functions, and our findings suggested that these functions are adequate for modeling the distance-dependent detectability of trees with PLS.

The choice of hazard rate detection function without series adjustments was determined using the minimum AIC. However, particularly in the case of stand 30k, the differences in AIC values (ΔAIC) were occasionally marginal. For instance, ΔAIC was 0.6 for the hazard rate function without series adjustments compared to the half-normal function with cosine adjustments. Akaike's rule of thumb is that two models are essentially indistinguishable if $\Delta AIC \leq 2$, that $2 < \Delta AIC \leq 4$ indicates moderate evidence of a difference in the models, and that $\Delta AIC > 4$ indicates strong evidence of a difference in the models. When the model selection is uncertain, we recommend adhering to a simpler model because it is easier to explain and less susceptible to issues with shape constraints that may arise when employing series expansions. Therefore, though the AIC for the half-normal function with cosine adjustments was slightly lower than that for the hazard rate function without series adjustments, we would still prefer the latter model.

Possible further model developments

Omission errors in proximity to the tran-

Tab. 5 - Accuracy of tree detection within sample line-plots of optimal width $2\omega_{opt}$.

Stand	BuLae	30k
Plot width, $2\omega_{opt}$ (m)	5.72	6.66
Omission error, o (%)	0.91	0.78
Commission error, c (%)	0.21	0.39
Detection rate, d_r (%)	99.07	99.23
Overall accuracy, acc (%)	98.88	98.83

sect were minimal, justifying the use of the classic line transect sampling approach. The principal advantage of this method is its ability to self-adjust to different sighting conditions using flexible detection functions. Thus, the method can be applied to other research areas without the need for intense reference data collection.

The virtual absence of omission errors in close proximity to the transect may appear unexpected, because significant omission errors were observed near the scanner using single-scan TLS and the same point cloud processing algorithms (Ritter et al. 2020). However, PLS offers a significant advantage by scanning not only from a single point, but also along a line, thereby avoiding considerable shadowing. If shadowing and non-detection occur near the transects during further investigation, a correction can be implemented for imperfect detectability that was originally developed for point-transect sampling in conjunction with TLS (Ritter et al. 2020). However, this approach requires reference data for model fitting and may have limited practical applicability.

We employed the classic line transect sampling approach exclusively to estimate the detection probability and, consequently, tree density. However, it is theoretically possible to regard each tree as a cluster of volume units with a cluster size, enabling the estimation of the total volume per hectare by multiplying the estimated cluster density by an estimate of the mean cluster size (Ritter & Saborowski 2012). Because the detection probability of large clusters may differ from that of smaller clusters, modeling the expected size of the detected clusters as a function of the distance-dependent detection probability can correct for the potential size bias. This correction addresses the issue that would arise if the mean cluster size was simply estimated as the sample mean of all observed clusters (Buckland et al. 2001). While this approach has proven successful in the context of deadwood sampling (Ritter & Saborowski 2012) and TLS in single-scan mode (Astrup et al. 2014), it has a fundamental limitation: the correction for non-detection is applicable only to tree density and total volume. Additional details, such as diameter distribution, spatial arrangement of trees, and resulting interactions, cannot be obtained using this analytical method. Consequently, our emphasis was on determining the optimal line-plot width because line-plots provide an opportunity to evaluate the aforementioned supplementary information.

Possible areas of application

Many NFIs utilize systematically arranged clusters of multiple measurement units. These clusters are typically spaced several kilometers apart and require field crews to commute between them by car. However, the gaps between the measuring units within a cluster are considerably smaller,

necessitating field crews to walk these distances. For instance, the distances between measuring units within a cluster were 120 ft (36.58 m) in the US NFI (McRoberts et al. 2005), 150 m in the German NFI (Kändler 2009), 200 m in the Austrian NFI (Schadauer et al. 2007), and 250-450 m (depending on the ecoregion) in the Finnish NFI (Tomppo 2009). This study demonstrates the applicability of PLS to line-plots of comparable length (102.7-461.0 m). The field operator was required to carry the PLS system while walking along a line through the forest and pressing the instrument's start/stop button at the beginning and end of the transect. Consequently, we believe that it is feasible to integrate PLS-based line-plot sampling into existing large-scale forest inventories without requiring additional time in the field.

This study was constrained by the limited representation of the observed forest types, as it focused only on two stands. Consequently, further research should be conducted to investigate how various stand types and vegetation conditions (foliated versus defoliated) influence the detection function. The effectiveness of employing a global model adjusted for local visual conditions through the inclusion of covariates, compared with utilizing independent models tailored to specific areas, remains uncertain. Despite these ambiguities and considering the long-standing success of distance sampling, we contend that overcoming these challenges is feasible. Extending the method to diverse conditions is plausible for determining the optimal plot width for accurate assessment.

Conclusion

The distance sampling framework proved to be suitable for determining the optimum width for line-plots to be sampled with PLS, such that non-detection errors on these plots could be virtually eliminated (<1%). *A posteriori* segmentation of the line-plots into smaller units evidently reduced the standard error. This enabled the application of PLS to line-plots and ensured the accurate and precise estimation of tree density, basal area, and volume. Further investigations are required to validate these findings in various forest types. Nonetheless, we are confident that the methodology introduced in this study allows the integration of PLS-based line-plot sampling into existing forest inventories relying on systematically aligned sample plots. In the field, crews can seamlessly carry the PLS device while moving between sampling points, facilitating additional data collection without extending working hours.

References

Astrup R, Ducey MJ, Granhus A, Ritter T, Von Lüpke N (2014). Approaches for estimating stand-level volume using terrestrial laser scanning in a single-scan mode. *Canadian Journal of Forest Research* 44 (6): 666-676. - doi: [10.1139/cjfr-2013-0535](https://doi.org/10.1139/cjfr-2013-0535)

Bäuerle H, Nothdurft A (2011). Spatial modeling of habitat trees based on line transect sampling and point pattern reconstruction. *Canadian Journal of Forest Research* 41: 715-727. - doi: [10.1139/x11-004](https://doi.org/10.1139/x11-004)

Bauwens S, Bartholomeus H, Calders K, Lejeune P (2016). Forest inventory with terrestrial LiDAR: a comparison of static and hand-held mobile laser scanning. *Forests* 7 (6): 127. - doi: [10.3390/f7060127](https://doi.org/10.3390/f7060127)

Buckland ST, Anderson DR, Burnham KP, Laake JL, Borchers DL, Thomas L (2001). *Introduction to distance sampling: estimating abundance of biological populations*. Oxford Univ. Press, Oxford, UK, pp. 432. - doi: [10.1093/oso/9780198506492.001.0001](https://doi.org/10.1093/oso/9780198506492.001.0001)

Buckland ST, Anderson DR, Burnham KP, Laake JL, Borchers DL, Thomas L (2004). *Advanced distance sampling: estimating abundance of biological populations*. Oxford Univ. Press, Oxford, UK, pp. 416. [online] URL: <http://books.google.com/books?id=hBRREAAAQBAJ>

Chen S, Liu H, Feng Z, Shen C, Chen P (2019). Applicability of personal laser scanning in forestry inventory. *PLoS One* 14: e0211392. - doi: [10.1371/journal.pone.0211392](https://doi.org/10.1371/journal.pone.0211392)

Cochran WG (1977). *Sampling techniques*. John Wiley and Sons, New York, USA, pp. 428.

Dassot M, Constant T, Fournier M (2011). The use of terrestrial LiDAR technology in forest science: application fields, benefits and challenges. *Annals of Forest Science* 68: 959-974. - doi: [10.1007/s13595-011-0102-2](https://doi.org/10.1007/s13595-011-0102-2)

De Vries PG (1986). *Sampling theory for forest inventory: a teach-yourself course*. Springer, Berlin and Heidelberg, Germany, pp. 399.

Del Perugia B, Giannetti F, Chirici G, Travaglini D (2019). Influence of scan density on the estimation of single-tree attributes by hand-held mobile laser scanning. *Forests* 10: 277. - doi: [10.3390/f10030277](https://doi.org/10.3390/f10030277)

Didas CM (2009). *Sampling and classification of tree holes within a Northeast temperate forest system*. Master's Thesis, University of New Hampshire, Durham, USA, pp. 78. [online] URL: <http://scholars.unh.edu/thesis/444/>

Ducey MJ, Astrup R (2013). Adjusting for non-detection in forest inventories derived from terrestrial laser scanning. *Canadian Journal of Remote Sensing* 39: 410-425. - doi: [10.5589/m13-048](https://doi.org/10.5589/m13-048)

GeoSLAM (2023a). *GeoSLAM Hub*. Web site. [online] URL: <http://geoslam.com/hub/>

GeoSLAM (2023b). *GeoSLAM ZEB-HORIZON 3D*. Web site. [online] URL: <http://geoslam.com/solutions/zeb-horizon/>

Gollob C, Ritter T, Nothdurft A (2020). Forest inventory with long range and high-speed Personal Laser Scanning (PLS) and Simultaneous Localization and Mapping (SLAM) technology. *Remote Sensing* 12 (9): 1509. - doi: [10.3390/rs12091509](https://doi.org/10.3390/rs12091509)

Gollob C, Ritter T, Wassermann C, Nothdurft A (2019). Influence of scanner position and plot size on the accuracy of tree detection and diameter estimation using terrestrial laser scanning on forest inventory plots. *Remote Sensing* 11 (13): 1602. - doi: [10.3390/rs11131602](https://doi.org/10.3390/rs11131602)

Hyypä E, Muhojoki J, Yu X, Kukko A, Kaartinen H, Hyypä J (2021). Efficient coarse registration method using translation- and rotation-invari-

- ant local descriptors towards fully automated forest inventory. *ISPRS Open Journal of Photogrammetry and Remote Sensing 2* (Part 3/ W52): 100007. - doi: [10.1016/j.ophoto.2021.100007](https://doi.org/10.1016/j.ophoto.2021.100007)
- Kändler G (2009). The design of the second German National forest inventory. In: *Proceedings of the "8th Annual Forest Inventory and Analysis Symposium"* (McRoberts RE, Reams GA, Van PC D, McWilliams WH eds). Monterey (CA, USA) 16-19 Oct 2006. USDA Forest Service, Washington, DC, USA, pp. 408. [online] URL: <http://www.researchgate.net/publication/228948917>
- Kangas A, Gove JH, Scott CT (2006). Introduction. In: *"Forest Inventory - Methodology and Applications"* (Kangas A, Maltamo M eds). Springer, Dordrecht, Netherlands, pp. 362. - doi: [10.1007/1-4020-4381-3_1](https://doi.org/10.1007/1-4020-4381-3_1)
- Kauffman JB, Arifanti VB, Basuki I, Kurnianto S, Novita N, Murdiyarto D, Donato DC, Warren MW (2017). Protocols for the measurement, monitoring, and reporting of structure, biomass, carbon stocks and greenhouse gas emissions in tropical peat swamp forests. Center for International Forestry Research - CIFOR, Bogor, Indonesia, pp. 44. - doi: [10.17528/cifor/006429](https://doi.org/10.17528/cifor/006429)
- Kershaw JA, Ducey MJ, Beers TW, Husch B (2016). *Forest mensuration* (5th edn). John Wiley and Sons, New York, USA, pp. 613. - doi: [10.1002/9781118902028](https://doi.org/10.1002/9781118902028)
- Kissa DO, Sheil D (2012). Visual detection based distance sampling offers efficient density estimation for distinctive low abundance tropical forest tree species in complex terrain. *Forest Ecology and Management* 263: 114-121. - doi: [10.1016/j.foreco.2011.09.020](https://doi.org/10.1016/j.foreco.2011.09.020)
- Köhl M, Magnussen S (2016). Sampling in forest inventories. In: *"Tropical Forestry Handbook (2nd edn)"* (K Pancel, M Köhl eds). Springer, Berlin and Heidelberg, Germany, pp. 3633. - doi: [10.1007/978-3-642-54601-3_72](https://doi.org/10.1007/978-3-642-54601-3_72)
- Liang X, Kankare V, Hyyppä J, Wang Y, Kukko A, Haggrén H, Yu X, Kaartinen H, Jaakkola A, Guan F, Holopainen M, Vastaranta M (2016). Terrestrial laser scanning in forest inventories. *ISPRS Journal of Photogrammetry and Remote Sensing* 115: 63-77. - doi: [10.1016/j.isprsjprs.2016.01.006](https://doi.org/10.1016/j.isprsjprs.2016.01.006)
- Liang X, Hyyppä J, Kaartinen H, Lehtomäki M, Pyörälä J, Pfeifer N, Holopainen M, Brolly G, Francesco P, Hackenberg J, Huang H, Jo HW, Katoh M, Liu L, Mokroš M, Morel J, Olofsson K, Poveda-Lopez J, Trochta J, Wang D, Wang J, Xi Z, Yang B, Zheng G, Kankare V, Luoma V, Yu X, Chen L, Vastaranta M, Saarinen N, Wang Y (2018). International benchmarking of terrestrial laser scanning approaches for forest inventories. *ISPRS Journal of Photogrammetry and Remote Sensing* 144: 137-179. - doi: [10.1016/j.isprsjprs.2018.06.021](https://doi.org/10.1016/j.isprsjprs.2018.06.021)
- McRoberts RE, Bechtold WA, Patterson PL, Scott CT, Reams GA (2005). The enhanced forest inventory and analysis program of the USDA Forest Service: historical perspective and announcement of statistical documentation. *Journal of Forestry* 103 (6): 304-308. - doi: [10.1093/jof/103.6.304](https://doi.org/10.1093/jof/103.6.304)
- Miller DL, Rexstad E, Thomas L, Marshall L, Laake JL (2019). Distance sampling in R. *Journal of Statistical Software* 89 (1): 1-28. - doi: [10.18637/jss.v089.i01](https://doi.org/10.18637/jss.v089.i01)
- Mokroš M, Mikita T, Singh A, Tomaščík J, Chudá J, Wezyk P, Kuelka K, Surovy P, Klimánek M, Zieba-Kulawik K, Bobrowski R, Liang X (2021). Novel low-cost mobile mapping systems for forest inventories as terrestrial laser scanning alternatives. *International Journal of Applied Earth Observation and Geoinformation* 104: 102512. - doi: [10.1016/J.JAG.2021.102512](https://doi.org/10.1016/J.JAG.2021.102512)
- Penman J, Gytarsky M, Hiraishi T, Krug T, Kruger D (2003). Good practice guidance for land use, land-use change and forestry. Institute for Global Environmental Strategies - IGES, Haya-ma, Japan, pp. 590. [online] URL: http://www.ipcc-nggip.iges.or.jp/public/gpplulucf/gpplulucf_files/GPG_LULUCF_FULL.pdf
- Pollanschütz J (1965). Eine neue Methode der Formzahl- und Massenbestimmung stehender Stämme - Neue Form- bzw. Kubierungsfunktionen und ihre Anwendung [A new method for determining the shape, number and mass of standing trunks - New shape or cubic functions and their application]. *Technical Report* 68, Forstliche Bundesversuchsanstalt, Mariabrunn, Germany, pp. 186. [in German]
- Prieto Gonzalez R, Thomas L, Marques TA (2017). Estimation bias under model selection for distance sampling detection functions. *Environmental and Ecological Statistics* 24: 399-414. - doi: [10.1007/s10651-017-0376-0](https://doi.org/10.1007/s10651-017-0376-0)
- Quang PX (1993). Nonparametric estimators for variable circular plot surveys. *Biometrics* 49: 837-852. - doi: [10.2307/2532203](https://doi.org/10.2307/2532203)
- R Core Team (2022). R: a language and environment for statistical computing, v. 4.2.2. The R Foundation for Statistical Computing, Vienna, Austria. [online] URL: <http://www.r-project.org/>
- Ritter T, Saborowski J (2012). Point transect sampling of deadwood: a comparison with well-established sampling techniques for the estimation of volume and carbon storage in managed forests. *European Journal of Forest Research* 131 (6): 1845-1856. - doi: [10.1007/s10342-012-0637-2](https://doi.org/10.1007/s10342-012-0637-2)
- Ritter T, Nothdurft A, Saborowski J (2013). Correcting the nondetection bias of angle count sampling. *Canadian Journal of Forest Research* 43 (4): 344-354. - doi: [10.1139/cjfr-2012-0408](https://doi.org/10.1139/cjfr-2012-0408)
- Ritter T, Saborowski J (2014). Efficient integration of a deadwood inventory into an existing forest inventory carried out as two-phase sampling for stratification. *Forestry* 87 (4): 571-581. - doi: [10.1093/forestry/cpu016](https://doi.org/10.1093/forestry/cpu016)
- Ritter T, Schwarz M, Tockner A, Leisch F, Nothdurft A (2017). Automatic mapping of forest stands based on three-dimensional point clouds derived from terrestrial laser-scanning. *Forests* 8 (8): 265. - doi: [10.3390/f8080265](https://doi.org/10.3390/f8080265)
- Ritter T, Gollob C, Nothdurft A (2020). Towards an optimization of sample plot size and scanner position layout for terrestrial laser scanning in multi-scan mode. *Forests* 11: 1-23. - doi: [10.3390/f110101099](https://doi.org/10.3390/f110101099)
- Ritter T, Gollob C, Nothdurft A (2021). Modelling the detection rate of terrestrial laser scanning in multi scan mode. In: *Proceedings of the "SilviLaser Conference 2021"*. Vienna (Austria) 28-30 Sep 2021, pp. 53-55. - doi: [10.34726/WIM.1913](https://doi.org/10.34726/WIM.1913)
- Schadauer K, Gschwantner T, Gabler K (2007). Austrian national forest inventory: caught in the past and heading toward the future. In: *Proceedings of the "7th Annual Forest Inventory and Analysis Symposium"* (McRoberts R, Reams G, Van P D, McWilliams W eds). Portland (OR, USA) 3-6 Oct 2005. USDA Forest Service, Washington, DC, USA, pp. 319.
- Seber GAF (1982). *The estimation of animal abundance and related parameters* (2nd edn). Macmillan, New York, USA, pp. 654.
- Thomas L, Buckland ST, Burnham KP, Anderson DR, Laake JL, Borchers DL, Strindberg S (2012). Distance sampling. In: *"Encyclopedia of Environmental Metrics"* (El-Shaarawi AH, Piegorisch WW eds). John Wiley and Sons, New York, USA. - doi: [10.1002/9780470057339.vad033.pub2](https://doi.org/10.1002/9780470057339.vad033.pub2)
- Tockner A, Gollob C, Kranitzer R, Ritter T, Nothdurft A (2022). Automatic tree crown segmentation using dense forest point clouds from Personal Laser Scanning (PLS). *International Journal of Applied Earth Observations and Geoinformation* 114: 103025. - doi: [10.1016/j.jag.2022.103025](https://doi.org/10.1016/j.jag.2022.103025)
- Tockner A (2024). treeX - Package for individual tree detection and tree segmentation from terrestrial LiDAR data. Web site. [online] URL: <http://github.com/anditockner/treeX>
- Tokola T (2006). Europe. In: *"Forest Inventory - Methodology and Applications"* (Kangas A, Maltamo M eds). Springer, Dordrecht, Netherlands, pp. 362. - doi: [10.1007/1-4020-4381-3_18](https://doi.org/10.1007/1-4020-4381-3_18)
- Tomppo E (2006). The Finnish national forest inventory. In: *"Forest Inventory - Methodology and Applications"* (A Kangas, M Maltamo eds). Springer, Dordrecht, Netherlands, pp. 362. [online] URL: <http://link.springer.com/content/pdf/10.1007/1-4020-4381-3.pdf#page=189>
- Tomppo E (2009). The Finnish National Forest Inventory. In: *Proceedings of the "8th Annual Forest Inventory and Analysis Symposium"* (McRoberts RE, Reams GA, Van PC D, McWilliams WH eds). Monterey (CA, USA) 16-19 Oct 2006. USDA Forest Service, Washington, DC, USA, pp. 408.
- Tupinambá-Simões F, Pascual A, Guerra-Hernández J, Ordóñez C, De Conto T, Bravo F (2023). Assessing the performance of a handheld laser scanning system for individual tree mapping a mixed forests showcase in Spain. *Remote Sensing* 15 (5): 1169. - doi: [10.3390/rs15051169](https://doi.org/10.3390/rs15051169)
- Witzmann S (2022). Development and evaluation of algorithms for the automatic marker-free registration of forest point clouds obtained from Personal Laser Scanning. Master / Diploma Thesis, University of Natural Resources and Life Sciences, Vienna, pp. 29. [online] URL: <http://permalink.obvsg.at/bok/AC16762598>
- Witzmann S, Matitz L, Gollob C, Ritter T, Kranitzer R, Tockner A, Stampfer K, Nothdurft A (2022). Accuracy and precision of stem cross-section modeling in 3D point clouds from TLS and caliper measurements for basal area estimation. *Remote Sensing* 14 (8): 1923. - doi: [10.3390/RS14081923](https://doi.org/10.3390/RS14081923)